J Nanopart Res (2020) 22: 267
https://doi.org/10.1007/s11051-020-05001-7

RESEARCH PAPER

Graphene influence on the structure, magnetic, and optical properties of rare-earth perovskite

Seham K. Abdel-Aal · Ahmed S. Abdel-Rahman

Received: 18 June 2020 / Accepted: 26 August 2020 / Published online: 1 September 2020

Abstract Perovskite-graphene nanocomposites of rare-earth $LaFeO_3$-rGO and $LaFeO_3$ nanoparticles are synthesized and characterized. The preparation was done by citrate sol-gel method. The structural characterization has been performed using XRD and FT-IR. Scanning electron microscope (SEM) and atomic force microscope (AFM) were used to analyze the morphology of the prepared nanocomposite. Vibrating sample magnetometer (VSM) was used to study the magnetic properties of the investigated samples. Introducing graphene to the structure results increase in M_S. Also, the optical and thermal properties have been measured and discussed, and the effect of graphene is observed where it decreases the band gap than reported for pure $LaFeO_3$ nanoparticles.

Keywords Graphene-perovskite nanocomposite · Magnetic properties · Thermal properties · Energy band gap

This article is part of the topical collection: Nanotechnology in Arab Countries, Guest Editor: Sherif El-Eskandarany

S. K. Abdel-Aal (✉) · A. S. Abdel-Rahman (✉)
Physics department, Faculty of Science, Cairo University, Giza 12613, Egypt
e-mail: seham@sci.cu.edu.eg
e-mail: asabry@sci.cu.edu.eg

Introduction

Perovskite materials have drowned interest nowadays due to its multifunctional applications. Otherwise, it is hybrid perovskite (Abdel-Aal et al. 2019; Abdel-Aal and Abdel-Rahman 2019; Mostafa et al. 2018; Abdel-Aal et al. 2017a, b; Abdel-Aal and Abdel-Rahman 2017; Mostafa et al. 2017a, b; Abdel-Aal 2017; Mondal et al. 2017; Mostafa et al. 2014) or oxide perovskite with the general formula ABO_3, where A and B are metal ions with different sizes and valances. The rare-earth perovskite of $LaFeO_3$ is one of the most perovskite widely used for multifunctional applications such as catalysis, magnetic materials, sensors, electrode materials in fuel cells, and optoelectronic devices (Phokha et al. 2014; Afifah and Saleh 2016; Tang et al. 2013; Peng et al. 2015; Abazari et al. 2014; Li et al. 2010; Yang et al. 2007; Thirumalairajan et al. 2012; Sathishkumar et al. 2016; De Vidales et al. 2014; Jyothi et al. 2014; Milanova et al. 2014; Lee et al. 2014; Treves 1965; Kaiwen et al. 2013; Cristóbal et al. 2016; Wei et al. 2009). Many methods have been reported for synthesizing $LaFeO_3$ such as sol-gel, co-precipitation, bull milling, sonochemical, and hydrothermal (Phokha et al. 2014; Tang et al. 2013; Abazari et al. 2014; Wei et al. 2009).

Graphene is a 2D carbon sheet with one atom carbon atom thickness. It is one of the thinnest materials in the world. Recently the preparation and characterization of graphene and graphene nanocomposites attract the attention of scientists. These nanocomposites can process new properties that exhibit multiple functionalities (Abdel-Aal et al. 2018; Abdel-Aal and Mohamed 2019; Jogender et al. 2020; Mandeep and Kakkar 2019; Mahmoudi et al. 2018; Selvakumar et al. 2018; Amolloa et al. 2019; Molaei and Kazeminezhad 2019). Where it has strong mechanical and chemical stability, good electrical conductivity, high chemical stability, and large specific surface area, therefore it has drawn a great deal of research interest for various applications.

Perovskites have been widely used in the fields of catalysis, sensing, optics, electronics, photovoltaics, and magnetics. However, some inherent shortcomings, such as low efficiency (external quantum efficiency, power conversion, efficiency, etc.) and poor stability (against ultraviolet light, water, oxygen, etc.), limit their practical applications. Downsizing the materials into nanostructures and incorporating rare-earth ions are effective means to improve their properties and broaden their applications (Zeng et al. 2020).

For the synergetic effect of these two promising materials, perovskite $LaFeO_3$ and graphene, we combine the perovskite $LaFeO_3$ into the graphene sheet; some physical properties were measured and discussed. In this work, the citrate sol-gel method (Chinie et al. 2005) was used to prepare perovskite $LaFeO_3$–doped reduced graphene oxide. The target of this work is to present the structural, magnetic, and optical changes in the properties of $LaFeO_3$ as loaded on reduced graphene oxide. The synthesized nanocomposite was characterized by transmission electron microscopy (TEM), scanning electron microscope (SEM), atomic force microscopy (AFM), and X-ray diffraction (XRD).

Experimental details

Synthesis

Chemicals used in this work are purchased from Merck with purity exceeds 98%, solution of reagent grade. Graphene oxide was produced from graphite powder by using the Hummer's method. The details of the synthesis process were described in our previous work (Abdel-Aal et al. 2018; Abdel-Aal and Mohamed 2019).

Preparation of $LaFeO_3$ nanoparticles

$La(NO_3)_3{\cdot}6H_2O$, $Fe(NO_3)_3{\cdot}9H_2O$, and citric acid $C_6H_8O_7{\cdot}H_2O$ were used in the preparation. The equimolar ratios of the metal nitrates are weighed according to the composition of $LaFeO_3$, 4.33 g of $La(NO_3)_3{\cdot}6H_2O$, and 4.04 g of $Fe(NO_3)_3{\cdot}9H_2O$ and then dissolved in deionized water. 3.843 g of citric acid is added to the nitrates. The solution is under constant stirring at temperature 70–80 °C. The resulting is a dark brown of LaFe-($C_6H_8O_7{\cdot}H_2O$) gel complex, which is turned into a yellowish color upon the calcination process. The perovskite-type $LaFeO_3$ was obtained by decomposition of the dry gel complex at temperature 600 °C for 4 h at rate 4 °C/min.

Preparation of $LaFeO_3$-rGO nanocomposite

$LaFeO_3$-rGO nanocomposite is prepared by the same above steps but adding 500 mg graphene oxide by micropipette drop by drop during the stirring process at temperature 70–80 °C. The color of the $LaFeO_3$-rGO nanocomposite is light brown darker than the pure one.

Characterization

The morphology of $LaFeO_3$-rGO nanocomposites is investigated using a scanning electron microscope (SEM) model number JSM 6510 LV JEOL. The transmission electron microscopy (TEM) was obtained on JEOL JEM-1230 electron microscope. The atomic force microscopy (AFM) was obtained on AFM-Agilent Technologies. The magnetic properties were measured by high-sensitive vibrating sample magnetometer measurements (VSM) model 7404 LAKESHORE at room temperature. The XRD powder diffraction data are collected using X-ray diffractometer SIEMENS D-5000 with CuKα radiation $\lambda = 1.54056$ Å, the measuring range (2θ) from 5° to 75°, step 0.02°. Optical properties measured by using UV-Vis absorption and diffuse reflectance spectrum (UV-Vis-NIR spectrophotometer type Jasco-V-570 spectrophotometer, Japan) were recorded at room temperature in the wavelength range 200–2000 nm.

Results and discussion

Structure characterization

Figure 1 shows the XRD of $LaFeO_3$ nanoparticles, $LaFeO_3$-rGO nanocomposite, graphene oxide GO, and graphene G. The XRD diffraction pattern of $LaFeO_3$ is marked by green, while the peaks of $LaFeO_3$-rGO is

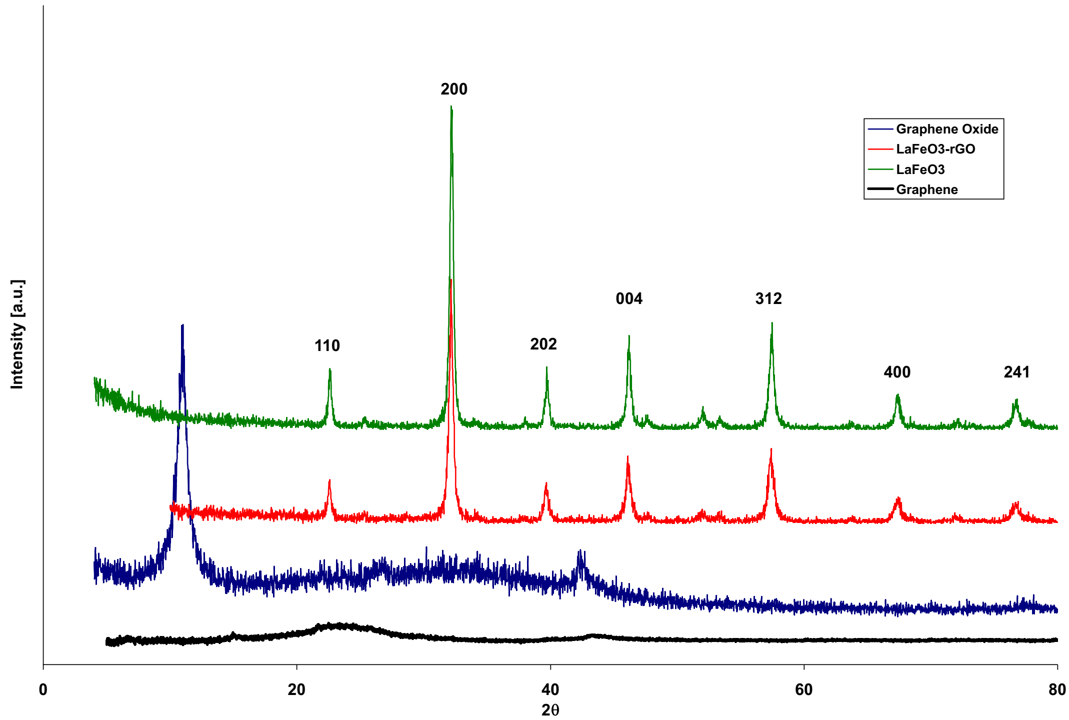

Fig. 1 XRD pattern of $LaFeO_3$, $LaFeO_3$-rGO, graphene oxide, and graphene

marked by red. Both are well defined, and it indicates that the synthesized nanocomposites are in a single phase. The XRD is indexed by an orthorhombic unit cell of $LaFeO_3$ without any impurity phases (reference

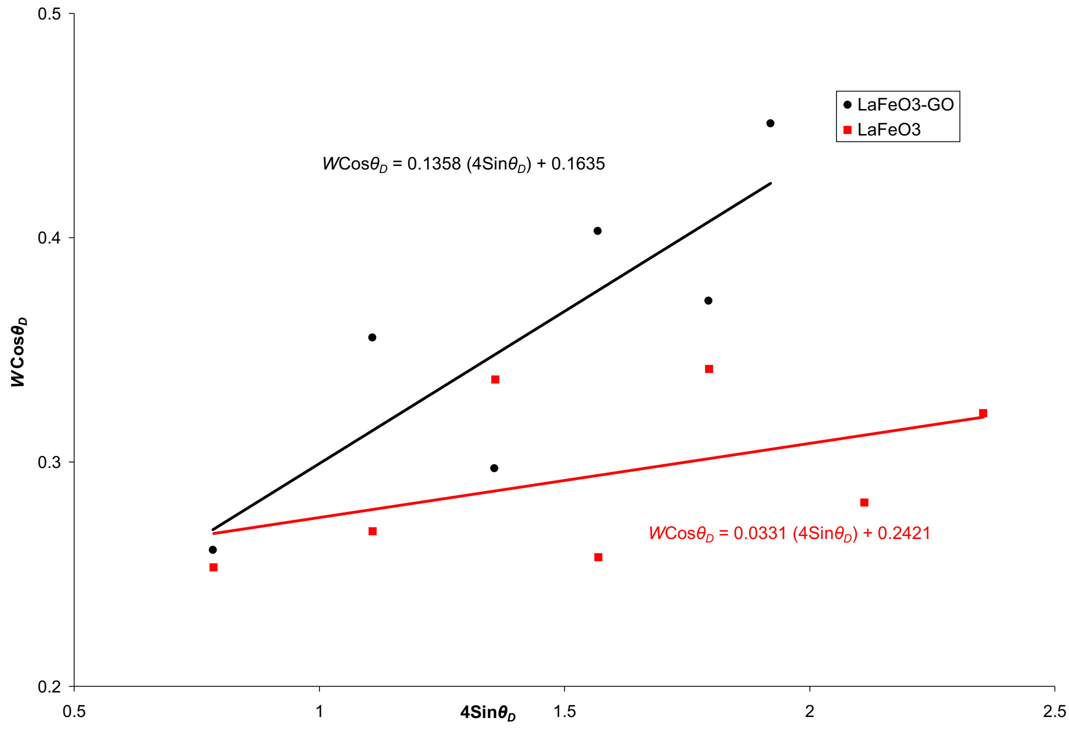

Fig. 2 Williamson-Hall Eq. (3) and its linear fit for $LaFeO_3$ and $LaFeO_3$-rGO nanocomposite

Table 1 Comparison between average crystalline sizes obtained from D_S Debye-Scherrer's and D_W Hall-Williamson's equations besides the lattice strain ε

	D_S (nm)	D_W (nm)	ε
$LaFeO_3$	49.87	59.81	0.03
$LaFeO_3$-rGO	41.99	88.59	0.14

code 01-080-3120). The values of the lattice parameters and the crystallite sizes are in good agreement with that of orthorhombic $LaFeO_3$ published elsewhere (Phokha et al. 2014; Afifah and Saleh 2016; Tang et al. 2013). Unlike the XRD powder diffraction pattern of graphene oxide GO (blue line), the perovskite $LaFeO_3$-rGO nanocomposite does not show any peak at $2\theta = 10$ in the XRD pattern. These results prove that the oxygen-containing groups of GO (COOH, OH, C=O) are removed and that most of GO are reduced hydrothermally into its reduced form rGO. Usually, the peak of rGO is week and broad as shown in Fig. 1. The diffraction pattern of $LaFeO_3$-rGO nanocomposite does not

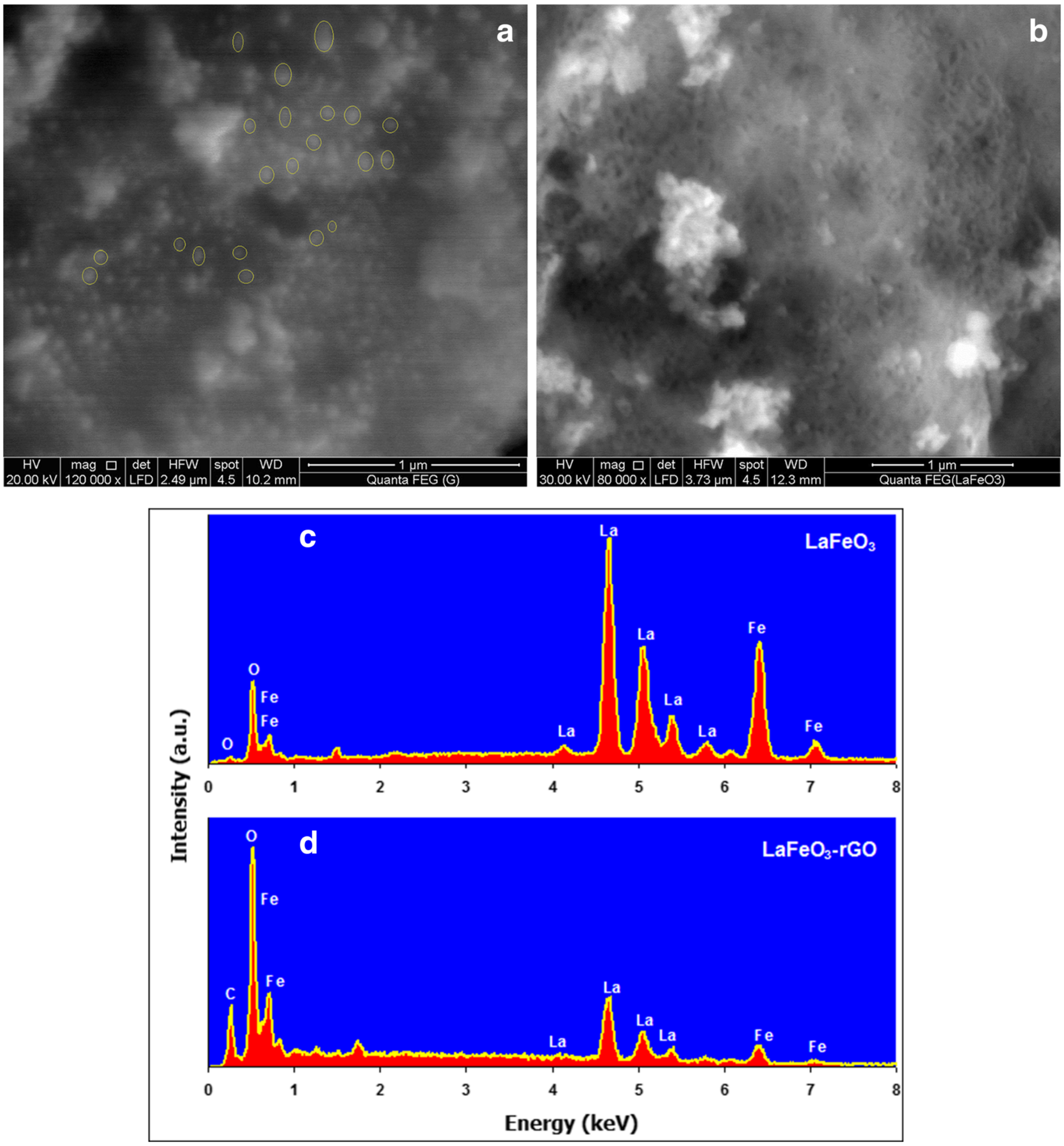

Fig. 3 **a** Scanning electron microscope image of $LaFeO_3$ nanoparticles. **b** Scanning electron microscope image of $LaFeO_3$-rGO nanocomposite. **c**, **d** EDX analysis of $LaFeO_3$ nanoparticles and $LaFeO_3$-rGO nanocomposite

Table 2 Elements composition of the $LaFeO_3$-rGO according to EDX data

Element	Weight (%)	Atomic (%)
C K	4.2	20.92
O K	8.94	33.41
Fe L	12.96	13.87
La L	73.9	31.8

contain the broad peak characteristic to rGO (2θ≈25°) due to high-intensity peaks of the crystalline $LaFeO_3$ as seen in Fig. 1.

The crystallite size can be calculated using the famous Debye-Scherrer's equation (Abdel-Aal et al. 2018; Abdel-Aal and Mohamed 2019):

$$W_f = 0.9\lambda/D\cos\theta_D \quad (1)$$

where λ is the wavelength of the used X-ray radiation ($\lambda_{Cu} = 1.54056$ Å), W_f is the width at half maximum intensity of the Bragg reflection excluding instrumental broadening, θ_D is the Bragg angle, and D is the average crystallize size.

The crystallites size and the average lattice strain ε can be estimated from the Williamson-Hall equation (Slimani et al. 2019; Almessiere et al. 2019; Abdel-Aal et al. 2020):

$$W = W_{strain} + W_f = 4\varepsilon\tan\theta_D + \frac{K\lambda}{D\cos\theta_D} \quad (2)$$

where W is the full-width half maximum of the XRD peaks, W_{strain} is the strain broadening which is uniform in all crystallographic directions, and $K = 0.94$ is the shape factor. When multiplying Eq. (2) by $\cos\theta_D$, it gives:

$$W\cos\theta_D = 4\varepsilon\sin\theta_D + \frac{K\lambda}{D} \quad (3)$$

Then, the relation between $W\cos\theta_D$ and $4\sin\theta_D$ will be a straight line (Fig. 2); the strain ε of the $LaFeO_3$ and $LaFeO_3$-rGO is deduced from the slope of linear fitting data, whereas the D is determined from the Y-intercept (Kλ/D).

The estimated values of D and ε deduced by using the Williamson-Hall equation are presented in Table 1. It is clear that the D value as calculated using the Williamson-Hall method is higher than that obtained using the Scherrer equation where the Williamson-Hall equation takes into consideration all diffraction peaks and assumes the brooding of it. That is related to the crystalline size as well as the lattice strain, which is not considered in the Scherrer equation (Slimani et al. 2019; Almessiere et al. 2019; Abdel-Aal et al. 2020). The large value of D from Williamson-Hall for $LaFeO_3$-rGO may be attributed to large lattice strain due to the addition of graphene.

Morphological characterization

Field emission scanning electron microscope FESEM

Figure 3 a and b show the SEM images of the $LaFeO_3$-rGO nanoparticles and $LaFeO_3$ nanocomposites, respectively. According to SEM images of $LaFeO_3$-rGO nanocomposites, spherical-shaped $LaFeO_3$ nanoparticles appear in a uniform

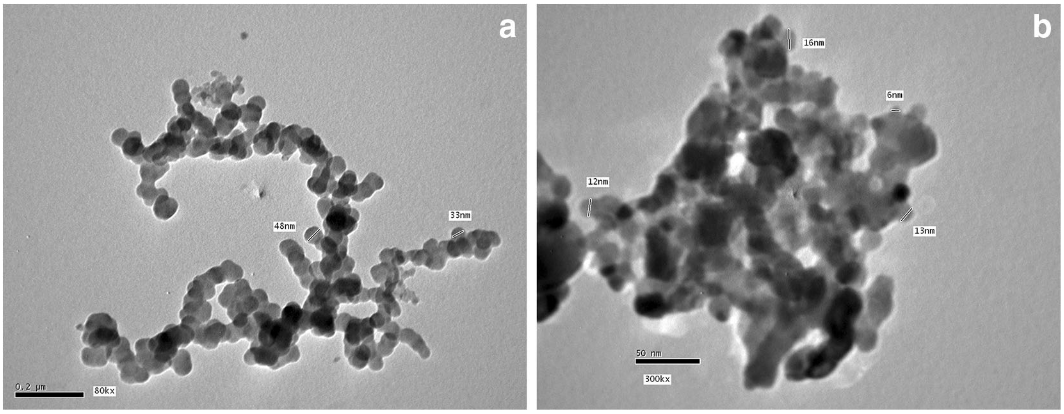

Fig. 4 **a** and **b** Transmission electron microscopy image of $LaFeO_3$-rGO perovskite nanocomposite

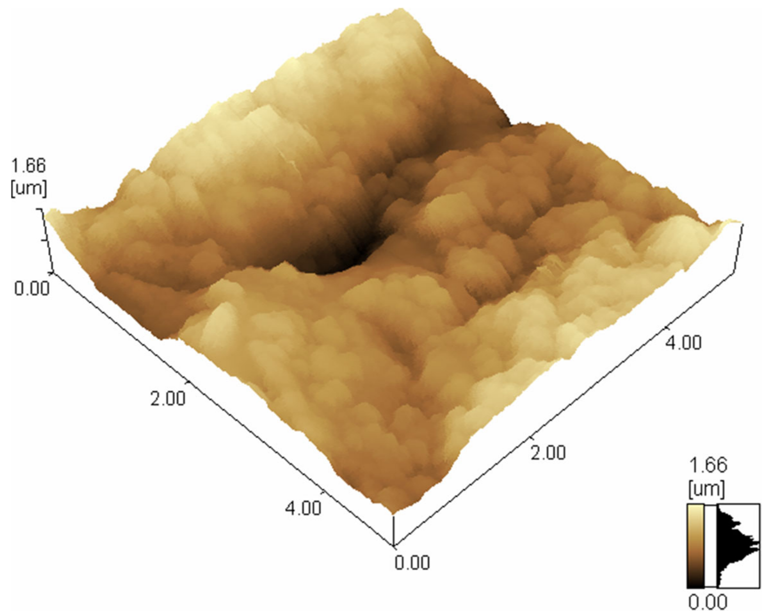

Fig. 5 AFM photo of $LaFeO_3$-rGO perovskite nanocomposite

distribution on the graphene sheets. The particle size is found from 45 to 37 nm with an average value of 41 nm which is in good agreement with the value obtained by Scherrer's equation. Figure 3 c and d show the energy dispersive X-ray analyses (EDX) of $LaFeO_3$ nanoparticles and $LaFeO_3$-rGO nanocomposites, respectively. The elemental composition of the $LaFeO_3$-rGO is shown in Table 2.

According to the atomic percentages of Fe and La in $LaFeO_3$-rGO, the EDX results show that a ratio of one Fe atom to one La atom, this is in good agreement with the structure of the $LaFeO_3$-rGO.

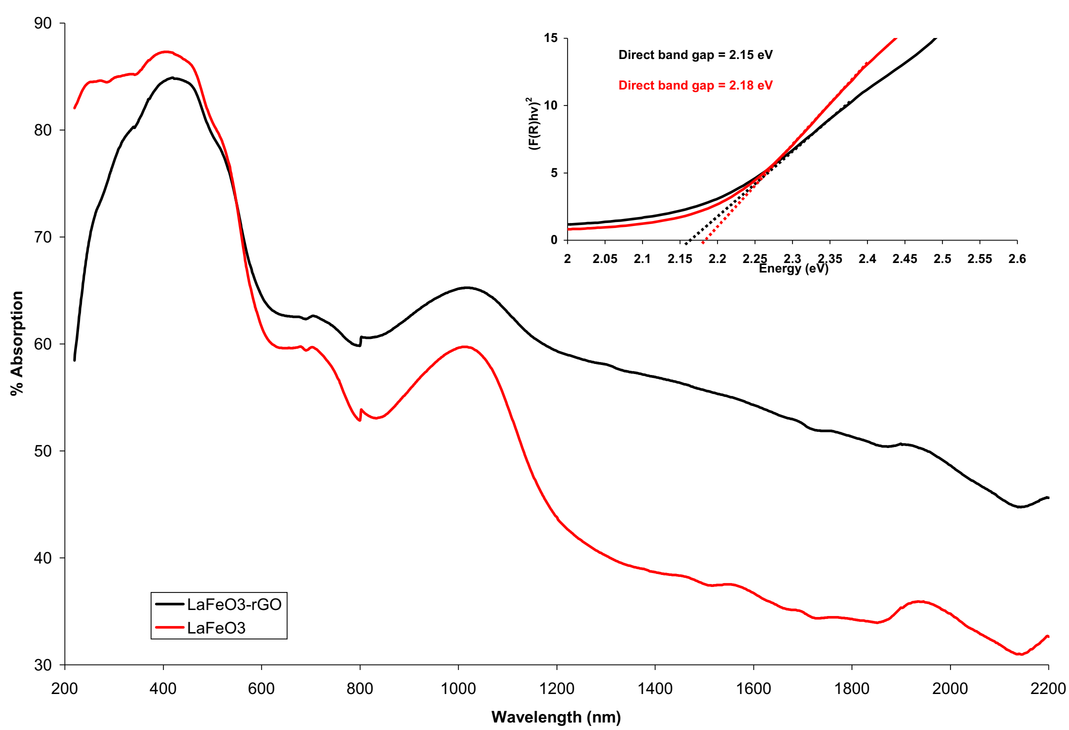

Fig. 6 The ultraviolet-visible spectra of $LaFeO_3$ and $LaFeO_3$-rGO. The inset figure is the band gap energy figure

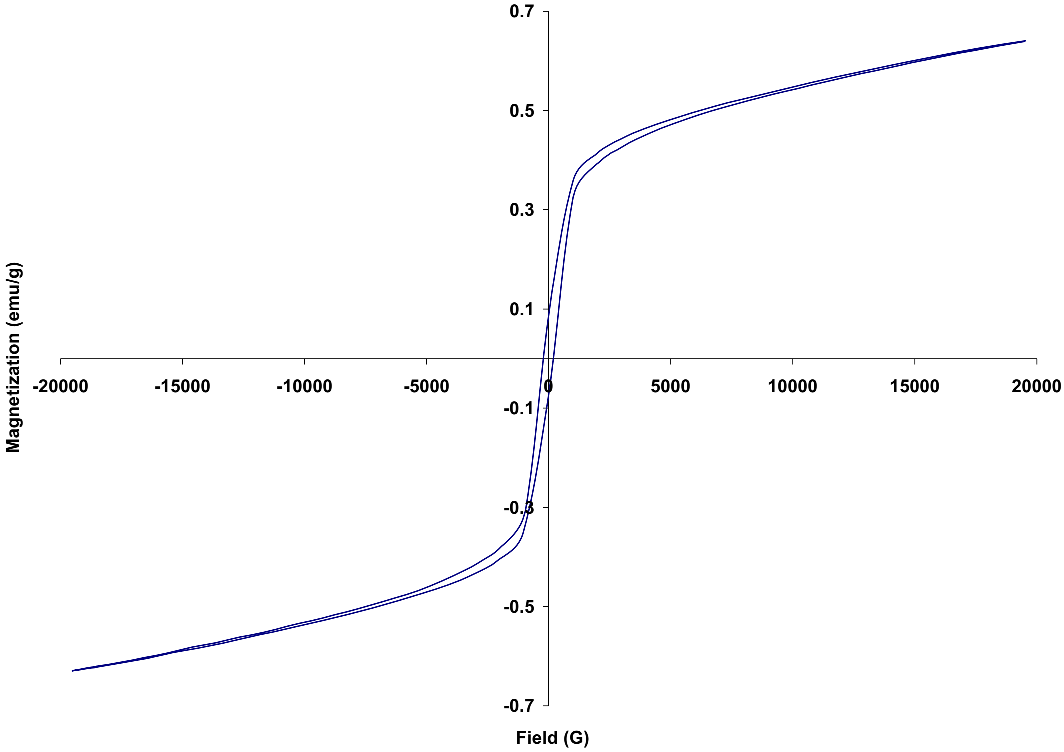

Fig. 7 VSM of $LaFeO_3$-rGO nanocomposites

Transmission electron microscopy TEM

Figure 4 a and b show the TEM images of the $LaFeO_3$-rGO nanoparticles at different magnifications. According to TEM images, the structure consists of a spherical shape of $LaFeO_3$ distributed on the graphene sheet. The particle size ranges from 33 to 48 nm.

Atomic force microscope AFM

The AFM picture captured to the surface of $LaFeO_3$-rGO perovskite nanocomposite is presented in Fig. 5. The analysis of the protrusions and pores results showed a distribution of Z_{max} and Z_{min} to be 50 nm and 36 nm, respectively. The surface roughness is 1.33. There are good agreements in particle size between XRD calculations (Debye-Scherrer and Hall-Williamson equations), SEM, and TEM photos where the particle size is about 42 nm.

Optical properties

The diffuse reflectance spectra (DRS) technique is used to study the optical properties of the synthesized samples based on the light reflection in the ultraviolet, visible, and near-infrared regions. The relation between the diffuse reflectance of the sample (R_∞), absorption (K), and scattering (S) coefficients is the Schuster-Kubelka-Munk remission function.

$$F_{SKM}(R_\infty) = \frac{(1-R_\infty)^2}{2R_\infty} = \frac{K}{S} \tag{4}$$

The extrapolating the straight line plot of $(F(R_\infty)\,h\nu)^n$ versus ($h\nu$) is used to determine the band gap E_g by knowing the used light frequency ν according to the following Kubelka-Munk equation:

$$(F(R_\infty)h\nu)^n = A\left(h\nu - E_g\right) \tag{5}$$

Table 3 The saturation magnetization, remnant magnetization, coercive field, energy loss, and squareness of $LaFeO_3$-rGO

Saturation magnetization	0.64 emu/g
Remnant magnetization	0.08 emu/g
H_c coercivity	192.6 G
Energy loss	460.23 erg/g
Squareness	0.1221

Table 4 Different preparation methods of $LaFeO_3$ nanoparticles, particle size, and saturation magnetization

Sample	Preparation method	Particle size (nm)	Saturation magnetization (emu/g)	Ref.
$LaFeO_3$	Polymerized complex	44.5	0.1	(Phokha et al. 2014)
	Sol-gel	21.9	0.38	(Saad et al. 2013)
	Milling	50	0.44	(Thuy and Minh 2012)
	Electrospining	20	0.9	(Lee et al. 2014)
$LaFeO_3$-rGO	Citrate sol-gel	41.9	0.64	This work

where A is a constant and h is the Plank's constant. The exponent n depends on the type of transition and can be used as $n = 1/2$ or 3/2 for indirect transitions and $n = 2$ or 3 for direct allowed transitions (Elseman et al. 2016). Figure 6 demonstrates the optical properties of the.

The electron excitation from the O^{2p} level (valence band) to Fe^{3d} level (conduction band) is responsible for strong ultraviolet-visible absorption for $LaFeO_3$-rGO nanocomposite in the optical properties showed in Fig. 6. This absorption is interesting because $LaFeO_3$-rGO could developed a new visible-light photocatalyst. The calculated band gap using Kubelka-Munk analysis is equals 2.18 eV for $LaFeO_3$, while graphene seems to reduce slightly the band gap energy of $LaFeO_3$-rGO to 2.15 eV as reported before and as shown in Fig. 6. This value is closed to the value reported in the literature (Phokha et al. 2014; Afifah and Saleh 2016).

Magnetic properties (VSM)

The magnetic properties of $LaFeO_3$ nanocomposite are investigated by vibrating sample magnetometer at room temperature, as shown in Fig. 7. The prepared nanocomposite shows weak antiferromagnetic behavior. The saturation magnetization, remnant magnetization, coercive field, energy loss, and squareness are tabulated in Table 3. This result is of great interest since bulk $LaFeO_3$ has antiferromagnetic behavior and may find application in the field of hyperthermia treatment. The incorporation of graphene layers seems does not change the magnetic nature of $LaFeO_3$.

Table 4 shows the different preparation methods of $LaFeO_3$ nanoparticles and their relation with particle size and saturation magnetization. It is seen that the saturation magnetization size, as well as particle, depending on the preparation conditions, the least particle size obtained by Lee et al. (Lee et al. 2014) by electrospinning method with the highest saturation

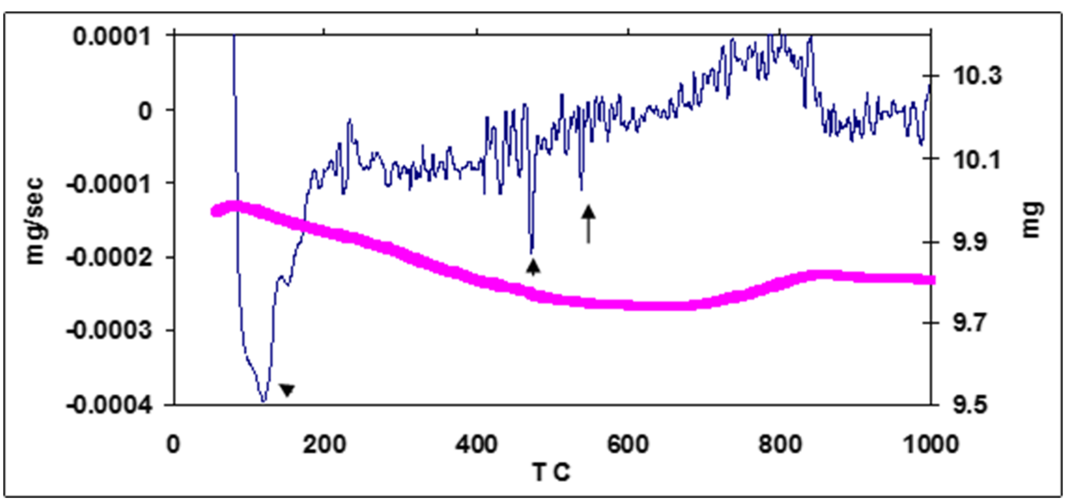

Fig. 8 TGA and DrTGA of $LaFeO_3$-rGO

magnetization observed. By introducing graphene, the particle size slightly increases (41.9 nm) due to the formation of islands of $LaFeO_3$ on the surface of the graphene sheet; the saturation magnetization is increased than recorded before (Phokha et al. 2014; Saad et al. 2013; Thuy and Minh 2012) for pure $LaFeO_3$ but less than the value recorded by electrospinning method. This may be attributed to the introduction of graphene into the structure which increases the magnetic moment interaction, thus increasing the magnetization.

Thermal properties

Figure 8 shows the thermal gravitational analysis (TGA) (pink line) and its derivative (black line) thermographs of $LaFeO_3$-rGO; three distinct wt loss steps are observed. These are accompanied by endothermic peaks around 123 °C, 472 °C, and 538 °C. The weight loss arises due to the loss of residual moisture in the powder suggesting the burnout of moisture, trapped solvent, and oxygen functional group of graphene oxide. No weight loss is observed above 600 °C indicates that the reaction is complete, and no evidence of a phase transition is present in the sample.

Conclusion

$LaFeO_3$ nanoparticles and $LaFeO_3$-rGO nanocomposite are successfully prepared by the citrate auto-combustion method. The characterization tools prove the formation of the desired materials in a single phase. The introduction of graphene into the structure $LaFeO_3$ decreases the particle size by ≈ 10 nm. Optical properties for both samples show strong absorption in the UV-Vis region. The graphene is also affected the energy band gap values by a slight decrease by 0.03 eV as well as increases the value of saturation magnetization. The thermal properties indicate the thermal stability of the prepared perovskite graphene nanocomposites over a long range of temperatures up to 1000 °C.

Acknowledgments The authors thank Dr. E. Atteia for providing some chemicals for the preparation process.

Compliance with ethical standards

Conflict of interest The authors declare that they have no conflict of interest.

References

Abazari R, Sanati S, Saghatforoush LA (2014) Mater Sci Semicond Process 25:301

Abdel-Aal SK (2017) Synthesis, characterization, thermal, and electrical properties of new diammonium hybrid perovskite [NH 3 -(CH 2) 7 -NH 3]CaCl 2 Br 2. Solid State Ionics 303: 29–36

Abdel-Aal SK, Abdel-Rahman AS (2017) Synthesis, structure, lattice energy and enthalpy of 2D hybrid perovskite [NH3(CH2)4NH3]CoCl4, compared to [NH3(CH2)nNH3]CoCl4, n=3–9. J Cryst Growth 457:282–288

Abdel-Aal SK, Abdel-Rahman AS (2019) Fascinating Physical properties of 2d hybrid perovskite [(NH3)(CH2)7(NH3)]CuClxBr4−x, x = 0, 2 and 4. J Electron Mater 48:1686–1693

Abdel-Aal SK, Mohamed SG (2019) Facile synthesis of Mn3O4-rGO nanocomposite as an efficient electrode material for application in supercapacitors. J Electron Mater 48:4977–4986

Abdel-Aal SK, Abdel-Rahman Ahmed S, Gamal Wafia M, Mohamed A-K, Ayoub HS, El-Sherif AF, Fawzy M, Bozhko S, Yakimov EE, Yakimov EB (2019) Acta Cryst B 75:880

Abdel-Aal SK, Abdel-Rahman AS, Kocher-Oberlehner G, Ionov A, Mozhchil RN (2017a) Structure, optical studies of two-dimensional hybrid perovskite for photovoltaic applications. Acta Cryst A 73:C1116

Abdel-Aal SK, Kocher-Oberlehner G, Ionov A, Mozhchil RN (2017b) Effect of organic chain length on structure, electronic composition, lattice potential energy, and optical properties of 2D hybrid perovskites [(NH3)(CH2) n (NH3)]CuCl4, n = 2–9. Appl Phys A Mater Sci Process 123:531

Abdel-Aal SK, Ionov A, Mozhchil RN, Naqvi AH (2018) Appl Phys A Mater Sci Process 124:365

Abdel-Aal SK, Abdel-Rahman AS, Ismail SH (2020) Egypt J Solids 43 accepted

Afifah N, Saleh R (2016) Synthesis, characterization and catalytic properties of perovskite lafeo3nanoparticles. J Phys Conf Ser 710:012030

Almessiere MA, Slimani Y, Güner S, Leusen J, van Baykal A, Kögerler P (2019) J Mater Sci Mater Electron 30:11181

Amolloa TA, Mola GT, Nyamori VO (2019) Sol Energy 171:83–91

Chinie AM, Stefan A, Georgescu S (2005) Romanian Rep Phys 57:412

Cristóbal A, Botta P, Bercoff P, López JP (2016) IOP Publ J Phys Conf Ser 710:012030

De Vidales MM, Barba S, Sáez C, Cañizares P, Rodrigo M (2014) Coupling ultraviolet light and ultrasound irradiation with conductive-diamond electrochemical oxidation for the removal of progesterone. Electrochim Acta 140:20–26

Elseman AM, Rayan DA, Rashad MM (2016) J Mater Sci Mater Electron 27:2652

Jogender M, Badhani B, Kakkar R (2020) Struct Chem. https://doi.org/10.1007/s11224-020-01552-6

Jyothi K, Yesodharan S, Yesodharan E (2014) Ultrasound (US), Ultraviolet light (UV) and combination (US+UV) assisted semiconductor catalysed degradation of organic pollutants in

water: oscillation in the concentration of hydrogen peroxide formed in situ. Ultrason Sonochem 21:1787–1796
Kaiwen Z, Xuehang W, Wenwei W, Jun X, Siqi T, Sen L (2013) Nanocrystalline LaFeO3 preparation and thermal process of precursor. Adv Powder Technol 24:359–363
Lee W, Yun HJ, Yoon J (2014) Characterization and magnetic properties of LaFeO3 nanofibers synthesized by electrospinning. J Alloys Compd 583:320–324
Li F, Liu Y, Liu R, Sun Z, Zhao D, Kou C (2010) Preparation of Ca-doped LaFeO3 nanopowders in a reverse microemulsion and their visible light photocatalytic activity. Mat Lett 64: 223–225
Mahmoudi T, Wang Y, Hahn Y-B (2018) Graphene and its derivatives for solar cells application. Nano Energy 47:51–65
Mandeep SL, Kakkar R (2019) ChemistrySelect 4:4967–4974
Milanova M, Zaharieva J, Todorovska R, Todorovsky D (2014) Polymetallic citric complexes as precursors for spray-pyrolysis deposition of thin LaFeO3 films. Thin Solid Films 562:43–48
Molaei P, Kazeminezhad I (2019) One-step in situ synthesis of antimony sulfide/reduced graphene oxide composite as an absorber layer with enhanced photocurrent performances for solar cells. J Nanopart Res 21:54
Mondal P, Abdel-Aal SK, Das D, Manirul IS (2017) Catal Lett 147:2332
Mostafa MF, Abdel-Aal Seham K, Tammam A (2014) Ind J Phys 88:49
Mostafa MF, El-khiyami SS, Abdel-Aal SK (2017a) Crystal structure, phase transition and conductivity study of two new organic – inorganic hybrids: [(CH2)7(NH3)2]X2, X = Cl/Br. J Mol Struct 1127:59–73
Mostafa MF, El Khiyami SS, Abdel-Aal SK (2017b) Discontinuous transition from insulator to semiconductor induced by phase change of the new organic- inorganic hybrid [(CH2)7(NH3)2]CoBr4. Mater Chem Phys 199: 454–463
Mostafa MF, El-khiyami SS, Abdel-Aal SK (2018) Structure, thermal, and impedance study of a new organic–inorganic hybrid [(CH 2) 7 (NH 3) 2]CoCl 4. J Phys Chem Solids 118:6–13
Peng Q, Shan B, Wen Y, Chen R (2015) Enhanced charge transport of LaFeO3 via transition metal (Mn, Co, Cu) doping for visible light photoelectrochemical water oxidation. Inter J Hydrogen Energy 40:15423–15431
Phokha S, Pinitsoontorn S, Maensiri S, Rujirawat S (2014) Structure, optical and magnetic properties of LaFeO3 nanoparticles prepared by polymerized complex method. J Sol-Gel Sci Tech 71:333–341
Saad AA, Khan W, Dhiman P, Naqvi AH, Singh M (2013) Structural, optical and magnetic properties of perovskite (La1−x Sr x)(Fe1−x Ni x)O3, (x = 0.0, 0.1 & 0. 2) nanoparticles. Electron Mater Lett 9:77–81
Sathishkumar P, Mangalaraja RV, Anandan S (2016) Review on the recent improvements in sonochemical and combined sonochemical oxidation processes – A powerful tool for destruction of environmental contaminants. Renew Sust Energ Rev 55:426–454
Selvakumar D, Murugadoss G, Alsalme A, Alkathiri AM, Jayavel R (2018) Heteroatom doped reduced graphene oxide paper for large area perovskite solar cells. Sol Energy 163:564–569
Slimani Y, Almessiere MA, Hannachi E, Baykal A, Manikandan A, Mumtaz M, Ben AF (2019) Influence of WO3 nanowires on structural, morphological and flux pinning ability of YBa2Cu3Oy superconductor. Ceram Int 45:2621–2628
Tang P, Tong Y, Chen H, Cao F, Pan G (2013) Microwave-assisted synthesis of nanoparticulate perovskite LaFeO3 as a high active visible-light photocatalyst. Curr Appl Phys 13: 340–343
Thirumalairajan S, Girija K, Ganesh I (2012) Controlled synthesis of perovskite LaFeO3 microsphere composed of nanoparticles via self-assembly process and their associated photocatalytic activity. Chem Engin J 209:420–428
Thuy NT, Minh DL (2012) Adv Mater Sci Eng 1155:380306
Treves D (1965) Studies on orthoferrites at the Weizmann Institute of Science. J Appl Phys 36:1033–1039
Wei Z, Xu Y, Liu H, Hu C (2009) Preparation and catalytic activities of LaFeO3 and Fe2O3 for HMX thermal decomposition. J Hazard Mater 165:1056–1061
Yang M, Xu A, Du H, Sun C, Li C (2007) J Hazard Mater B139: 86
Zeng Z, Xu Y, Zhang Z, Gao Z, Luo M, Yin Z, Zhang C, Xu J, Huang B, Luo F, Du Y, Yan C (2020) Rare-earth-containing perovskite nanomaterials: design, synthesis, properties and applications. Chem Soc Rev 49:1109–1143